

Discovery of Orally Bioavailable Purine-Based Inhibitors of the Low-Molecular-Weight Protein Tyrosine Phosphatase

Stephanie M. Stanford,* Michael A. Diaz, Robert J. Ardecky, Jiwen Zou, Tarmo Roosild, Zachary J. Holmes, Tiffany P. Nguyen, Michael P. Hedrick, Socorro Rodiles, April Guan, Stefan Grotegut, Eugenio Santelli, Thomas D. Y. Chung, Michael R. Jackson, Nunzio Bottini,* and Anthony B. Pinkerton*

 Cite This: *J. Med. Chem.* 2021, 64, 5645–5653

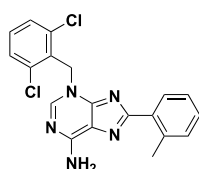
 Read Online

ACCESS |

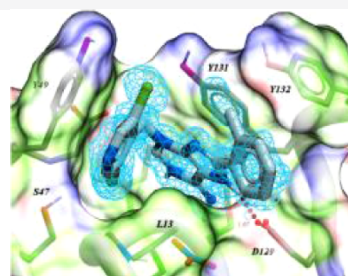
 Metrics & More

 Article Recommendations

 Supporting Information



5d
 LMPTP IC₅₀ = 0.020 μM
 >1000 fold selectivity vs other phosphatases



ABSTRACT: Obesity-associated insulin resistance plays a central role in the pathogenesis of type 2 diabetes. A promising approach to decrease insulin resistance in obesity is to inhibit the protein tyrosine phosphatases that negatively regulate insulin receptor signaling. The low-molecular-weight protein tyrosine phosphatase (LMPTP) acts as a critical promoter of insulin resistance in obesity by inhibiting phosphorylation of the liver insulin receptor activation motif. Here, we report development of a novel purine-based chemical series of LMPTP inhibitors. These compounds inhibit LMPTP with an uncompetitive mechanism and are highly selective for LMPTP over other protein tyrosine phosphatases. We also report the generation of a highly orally bioavailable purine-based analogue that reverses obesity-induced diabetes in mice.

INTRODUCTION

Patients with type 2 diabetes mellitus (T2DM) respond poorly to insulin, a condition known as insulin resistance.^{1,2} Insulin resistance is the underlying defect at the core of the metabolic syndrome/pre-diabetes that can develop into T2DM and is commonly found in obese and overweight individuals.^{1,2} Although currently, there are multiple anti-diabetic agents available, glycemic control is not sustained in many T2DM patients on these treatments.³ Thus, there is a major unmet medical need for insulin-sensitizing agents that would enable improved glycemic control in obese and overweight patients with T2DM.

Once insulin engages the insulin receptor (IR) on the surface of cells, the IR triggers a network of signal transduction pathways inside the cell through phosphorylation of itself and other substrates.^{4,5} These actions can be reversed by protein tyrosine phosphatases (PTPs) that regulate insulin signaling by dephosphorylating the IR. Thus, a proposed strategy for developing insulin sensitizers has been to target these PTPs.^{6,7} It has long been suggested that targeting the PTP 1B (PTP1B), which dephosphorylates the activation motif of the IR, would relieve insulin resistance and restore glucose tolerance.⁷ However, despite extensive validation of this and other PTPs, several structural features of these enzymes—including

a small, highly charged, and well-conserved active-site—have rendered them notoriously difficult to drug.⁸ In efforts to overcome this problem, novel approaches are being pursued, such as development of bidentate inhibitors of SH2 domain-containing phosphatase 2 (SHP2)⁹ and non-competitive allosteric inhibitors of PTP1B,¹⁰ SHP2,¹¹ and lymphoid phosphatase (LYP).¹²

Several lines of evidence suggest that the low-molecular-weight PTP (LMPTP) is a key driver of insulin resistance in obesity. LMPTP is a small (18 kDa), ubiquitously expressed cytosolic PTP encoded by the *ACPI* gene.¹³ Among the PTPs, LMPTP and the recently reclassified SSU72 are the only members of the class II subfamily of PTPs.^{14,15} *ACPI* encodes two isoforms—LMPTP-A and LMPTP-B—which are expressed as a result of alternative splicing of the same transcript.¹⁶ Genetic evidence in humans suggests that LMPTP promotes T2DM and insulin resistance since *ACPI* alleles

Received: December 9, 2020

Published: April 29, 2021



encoding low LMPTP enzymatic activity are associated with lower glycemic levels in diabetic and nondiabetic subjects.^{17–21} Knockdown of LMPTP expression by antisense oligonucleotides was reported to decrease insulin resistance in diet-induced obese (DIO) C57BL/6 (B6) mice and enhance IR phosphorylation in mouse hepatocytes and adipocytes.²² Through the use of global and tissue-specific LMPTP deletion in mice, we reported that LMPTP drives obesity-induced diabetes through an action on the liver and that LMPTP deletion increases liver IR phosphorylation in response to insulin.²³

Since LMPTP inhibitors would be highly valuable for studying the role of LMPTP in insulin resistance and other biological processes, we have sought to develop selective, orally bioavailable LMPTP chemical inhibitors. We previously reported the first orally bioavailable inhibitor of LMPTP activity, compound (compd) 23, which alleviates insulin resistance in DIO mice.²³ Here, we report the development of a novel, purine-based chemical series of LMPTP inhibitors that display substantially improved potency over the previously reported series and maintain high selectivity (>1000-fold) for LMPTP over other PTPs. Enzymatic studies and co-crystallization reveal that these compounds inhibit LMPTP through an uncompetitive mechanism of action (MOA) by binding at the opening of the active-site pocket. Structure–activity relationship (SAR) studies around this structure led to an orally bioavailable derivative with low nanomolar potency that, upon oral administration to DIO mice, increased liver IR phosphorylation and alleviated diabetes. Our findings reveal a novel chemical structure to inhibit LMPTP that can be utilized for biological studies and potentially for drug development efforts against this target.

RESULTS AND DISCUSSION

Identification of a Novel LMPTP Inhibitor Scaffold.

We previously reported a novel chemical series of LMPTP inhibitors, exemplified by the National Institutes of Health (NIH) probe ML400 and orally bioavailable derivative compd 23 (1; Figure 1).^{23,24} This series was derived from a quinoline

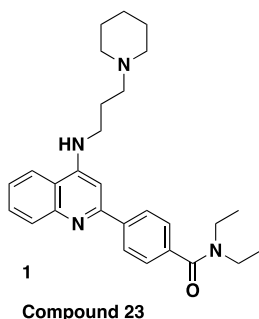


Figure 1. Chemical structure of previously reported LMPTP inhibitor compd 23 (1).

core-based scaffold that emerged from high-throughput screening (HTS) of small-molecule compounds from the NIH Molecular Libraries Small Molecule Repository.^{23,24} From this HTS, we also identified additional hit MLS-0045954 (2; Figure 2), which had an unrelated, purine-based scaffold.²³ Interestingly, LMPTP has previously been reported to be activated by purine biomolecules such as adenine and cyclic guanosine monophosphate.¹³ Since 2 displayed high

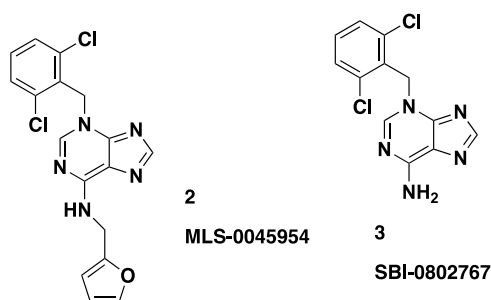


Figure 2. Chemical structures of purine-based LMPTP inhibitors.

selectivity for LMPTP over PTPs LYP and vaccinia H1-related phosphatase (VHR) in our HTS workflow,²³ we decided to explore further development of this scaffold.

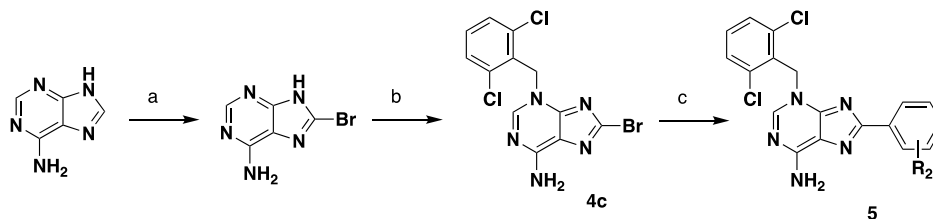
Chemistry. The compounds described in this paper consist of a purine core structure with an N-linked benzyl group off the 3 position and (in most cases) substitution at the 8 position. A representative synthesis is shown in Scheme 1. Starting from 6-aminopurine, bromination was followed by benzylation to give 4c. In the case of unsubstituted aminopurines, a mixture of benzylation products was obtained, from which intermediates such as 4c could be readily separated albeit in lower yields. For larger scale syntheses, we first protected the free NH₂ with a PMB group. Benzylation of the PMB-protected aminopurine proceeded regioselectively and in high yield. Compd 4c could be coupled with the appropriate boronic acid to give a range of final compounds (for full synthetic details see the Supporting Information).

Structure–Activity Relationship. For our primary SAR-driven assay, we used the same biochemical assay that was deployed for the HTS.²³ Counterscreens against VHR and LYP were performed routinely; in all cases, we saw no cross-reactivity. Our preliminary SAR around 2 showed that substitution off the 6-amino group was not preferred (data not shown). Indeed, the unsubstituted 3 was >10 fold more potent than 2 and therefore became our starting point for additional SAR studies (Figure 2 and Table 1). We assessed the selectivity of 3 against a panel of PTPs, including LMPTP and class I tyrosine-specific and dual-specific PTPs. This compound was remarkably selective for LMPTP as at a concentration of 40 μM (more than 100× the IC₅₀), no other PTP tested was inhibited by 50% (Figure S1).

We initially focused on exploring substitution off the 8 position (Table 1). Halogens were not well tolerated (4c and 4d). A potency similar to that of 3 was observed with a methyl group (4a). A significant increase in potency was seen with phenyl substitution (4b); we therefore decided to fully explore phenyl substitution (Table 2).

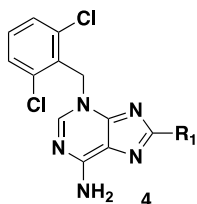
Most phenyl substituents were tolerated, but improved potency over the unsubstituted analogue is observed in only one case (the *ortho*-methyl analogue 5d). In general, there is a slight (~2–4 fold) preference for *ortho* substitution over *meta* and *para* (see, e.g., 5a vs 5b/c, 5d vs 5e/f and 5g vs 5h) with the exception being the *para*-fluoro analogue 5i.

Lastly, we examined substitution of the benzyl substituent off the 3-position (Table 3). 2,6-Bisubstitution was highly preferred compared to decreased potency with an unsubstituted ring (6a), mono-Cl derivatives (6b, 6d, or 6e), or 2,4-dichloro substitution (6c). 2-6-Dimethyl is tolerated (6f) albeit with a 10-fold loss in potency. A wide range of other substitutions were examined with complete loss of LMPTP

Scheme 1. Representative Synthesis of Purine Compounds^a

^aReagents and conditions: (a) Br₂, H₂O, rt, 60%; (b) K₂CO₃, DMF, rt, 36%; (c) Pd(dppf)Cl₂, dioxane/H₂O, 90 °C, 22–55%.

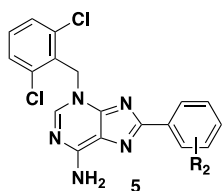
Table 1. Structures and LMPTP Activities of Analogues 4



compd #	R ₁	IC ₅₀ , μM ^a
3	H	0.239 ± 0.053 (72)
4a	–CH ₃	0.306 ± 0.017 (2)
4b	–Ph	0.104 ± 0.013 (4)
4c	–Br	17.6 ± 3.3 (2)
4d	–Cl	27.8 ± 6.8 (2)

^aMean ± SEM (*n*).

Table 2. Structures and LMPTP Activities of Analogues 5



compd #	R ₂	IC ₅₀ , μM ^a
5a	2-Cl	0.171 ± 0.010
5b	3-Cl	0.380 ± 0.053
5c	4-Cl	0.288 ± 0.008
5d	2-CH ₃	0.020 ± 0.005
5e	3-CH ₃	0.087 ± 0.003
5f	4-CH ₃	0.119 ± 0.014
5g	2-F	0.147 ± 0.037
5h	3-F	0.239 ± 0.008
5i	4-F	0.117 ± 0.008
5j	2-OCH ₃	0.106 ± 0.006
5k	2-CN	0.245 ± 0.050

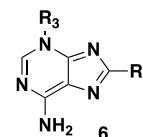
^aMean ± SEM (*n* = 4).

inhibition in most cases (data not shown). One exception was nitrogen incorporation in the ring (6g), which gives a threefold boost in potency. Combining this finding with the *ortho*-methylphenyl group (6h) gives an additional boost in potency.

We assessed the selectivity profile of 5d, the most potent of the analogue 5 compounds. We observed the same remarkable selectivity for LMPTP even at a concentration of 40 μM 5d (Figure S2). These data indicate that 5d is >1000× selective for LMPTP over all other PTPs tested.

Mechanism of Action. We examined the inhibitory MOA of 5d on LMPTP using *in vitro* kinetic analysis in the presence of increasing concentrations of an inhibitor. As shown in

Table 3. Structures and LMPTP Activities of Analogues 6



Compd #	R ₃	R ₄	IC ₅₀ , μM ^a
6a		–H	13.6 ± 0.4
6b		–H	1.93 ± 0.16
6c		–H	1.02 ± 0.01
6d		–H	18.5 ± 4.8
6e		–H	19.4 ± 2.2
6f		–H	3.43 ± 0.32
6g		–H	0.083 ± 0.006
6h			0.006 ± 0.001 (12)

^aMean ± SEM (*n* = 4 unless otherwise noted).

Figure 3, our data reveal an uncompetitive mechanism of inhibition. Fitting to a mixed model inhibition equation revealed a higher affinity of 5d for substrate-bound LMPTP than free LMPTP, as evidenced by the K_i'/K_i ratio (α) of 0.147 ± 0.104 , indicative of an uncompetitive binding mechanism (Figure 3a).^{25,26} Concomitant with this, Lineweaver–Burk analysis of the data resulted in the parallel plots characteristic of uncompetitive inhibition (Figure 3b).^{25,26} In further support of this, hydrolysis of the substrate by LMPTP exhibited decreasing V_{max} and decreasing K_m in the presence of increasing 5d concentrations (Figure 3c,d). Finally, since uncompetitive inhibitors exhibit increased inhibitory potency in the presence of increasing substrate,^{27,28} we assessed the potency of 5d at varying substrate concentrations. Consistent with an uncompetitive mechanism, 5d exhibited enhanced potency in the presence of increasing substrates (Figure 3e).

Co-crystallization and Structure of 5d Bound to LMPTP. We co-crystallized 5d with human LMPTP and solved the crystal structure of the complex to a resolution of

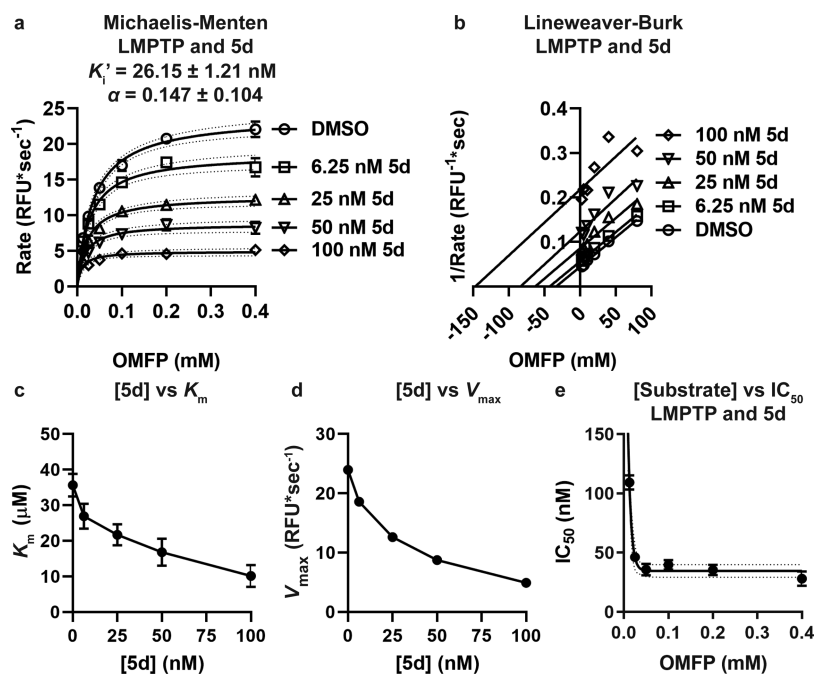


Figure 3. Analogue **5d** inhibits LMPTP with an uncompetitive MOA. (a,b) Activity of 20 nM human LMPTP-A on increasing concentrations of OMFP in the presence of increasing concentrations of **5d**. (a) Mean \pm SEM reaction rate vs OMFP concentration is shown. Lines show fitting to the Michaelis–Menten equation with a 95% confidence interval. Mean \pm SEM K_i' and α are shown. (b) Lineweaver–Burk plot of data from (a). Lines show fitting to a linear regression. (c,d) Mean \pm SEM K_m (c) and V_{max} (d) values for each concentration of inhibitor from the Michaelis–Menten curves in (a) are shown. (e) IC_{50} values were calculated for **5d** on 20 nM human LMPTP-A-catalyzed hydrolysis of increasing concentrations of OMFP. Mean \pm SEM IC_{50} from three independent experiments performed in triplicate is shown. Lines show fitting to the one-phase decay equation with a 95% confidence interval shown. (a–e) Data from three independent experiments performed in triplicate is shown.

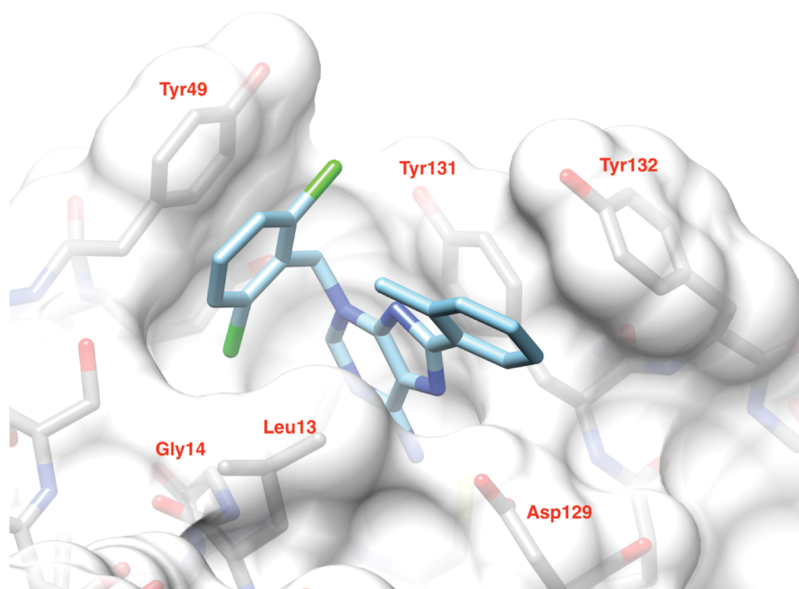


Figure 4. Crystal structure of **5d** with human LMPTP. Model of **5d** in the substrate binding site of LMPTP. The ligand is shown in light blue. The protein is shown as a solvent-accessible surface and stick representation (gray). Only one conformation of the *o*-tolyl group is shown for clarity. The figure was generated using Chimera.²⁹ PDB: 7KH8.

1.3 Å by molecular replacement. Crystals belong to Space Group $P2_12_12_1$ (see the [Experimental Section](#)) with two LMPTP molecules per asymmetric unit, related by a pseudodyad. They adopt similar conformations, with a root mean square deviation of 0.86 Å (all atoms) between them. Interpretable electron density was present for **5d** and for 155 residues in each of the two molecules, as detailed in the [Experimental Section](#). **5d** could be unambiguously modeled,

except for the *o*-tolyl group, which exists in two roughly equally populated conformations generated by a rotation of $\sim 60^\circ$ around the C8–C bond ([Figure S3](#)); as for one of them (shown in [Figure 4](#)) two copies could not simultaneously co-exist due to serious steric clashes across the non-crystallographic dyad, it is assumed to be the preferred one in solution and will be used in the discussion below.

Compd **5d** binds at the entrance of the catalytic pocket of LMPTP, with its aminopurine moiety approximately occupying the same region of space as the quinoline core in the previous crystal structure of a derivative of compd **18** bound to LMPTP.²³ When compared to compd **18** (PDB ID 5JNW), the aminopurine system still provides the bulk of the contacts with LMPTP by making a π - π aromatic stacking interaction with the side-chain of Tyr131 on one face, a hydrophobic interaction with Leu13 on the other, and a hydrogen bond with the carboxylate group of Asp129 via its N7; however, the presence of the primary amino group at position 6 adds a second hydrogen bond to the latter interaction (dashed lines in Figure S3). Unlike the aminopropyl piperidine group in **18**, the dichlorobenzyl ring binds tightly to a distal part of the active site, lying on a plane perpendicular to that of the purine group and displacing Tyr49 from a position it often occupies in other LMPTP structures. Here, it contributes a novel extensive π - π stacking interaction with the aromatic ring of Tyr49, while one of the chlorine atoms inserts into a pocket formed by Gly14 and the side-chains of Leu13, Ser47, Tyr49, Glu50, and the **5d** aminopurine ring (Figure S3), rationalizing the loss of potency upon its removal (Table 3). As expected from the SAR data, and likely as a consequence of constraints imposed by the dichlorobenzyl group, the *o*-tolyl ring is more solvent-exposed or involved in crystal contacts when compared to the cyanophenyl group in **18** (Figure S3). Its interaction with the protein is limited to one edge of the aromatic ring at a van der Waals distance from the side chains of Tyr132 and Asp129. Its methyl group however approaches the face of the dichlorophenyl group at a distance of 3.5 Å, which might explain the preference for ortho-substitution (Table 2). A nitrate ion from the crystallization buffer takes the place of the VO₃ group in 5JNW and mimics the presence of a phosphocysteine, consistent with the uncompetitive mechanism we observe (Figure S3). Interestingly, the mode of binding of **5d** closely resembles that of the LMPTP activator adenine in the yeast homologue LTP1³⁰ but with opposite effects due to a 180° rotation around the axis that runs through the center of the aromatic rings. While the adenine N3 points toward the active site and stabilizes a water molecule that is believed to be the nucleophile that attacks the phosphocysteine intermediate, the rearrangement we see in **5d** instead leads N6 to obstruct access to the active site, thus protecting the phosphocysteine from hydrolysis.

Pharmacokinetics. We examined a range of analogues for their rodent pharmacokinetics (PK) properties, with the results for **3**, **5d**, **6g**, and **6h** shown in Table 4 and the Supporting Information. The compounds without substitution on the 8 position (**3** and **6g**) showed low to moderate clearance and good oral bioavailability with modest (0.71 h for **6g**) or good (4.71 h for **3**) half-lives. In contrast, the two *ortho*-methylphenyl analogues (**5d** and **6h**) showed high clearance

Table 4. Selected Mouse PK Parameters for Compounds

compd ^a	Cl _p ^b (mL/min/kg)	V _d ^b (L/kg)	C _{max} ^c (ng/mL)	AUC ^c (ng·h/mL)	t _{1/2} ^c (h)	F %
3	5.8	3.01	5018	18544	4.71	66
5d	69	2.75	134	312	1.35	19
6g	18	0.81	8220	9501	0.71	100
6h	103	4.04	17	38	1.55	3

^aCompounds dosed 2 mpk IV and 10 mpk PO. ^bIV. ^cPO.

and modest to low oral bioavailability. In addition, **6g** showed only moderate plasma protein binding (88 and 89% bound in human and mouse plasma, respectively) and good microsomal stability (>90% remaining after 1 h of incubation in human and mouse liver microsomes). Due to the combination of potency and bioavailability, **6g** was selected for further in vitro and in vivo pharmacological profiling.

We confirmed that **6g** retains high selectivity (Figure 5) for LMPTP and an uncompetitive mechanism of LMPTP inhibition (Figure S4).

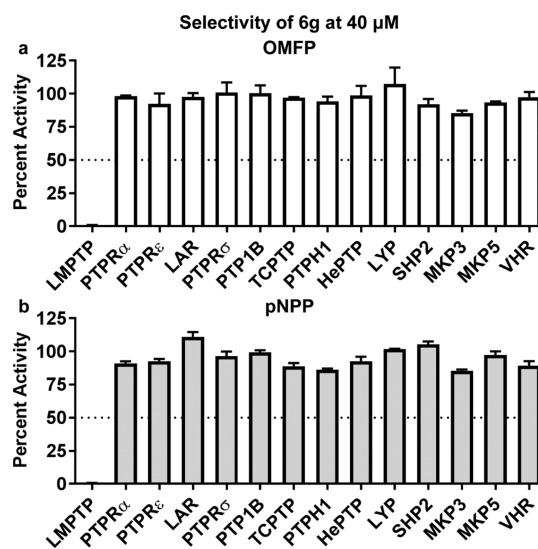


Figure 5. Selectivity of analogue **6g**. (a,b) PTPs were incubated with (a) 0.4 mM OMFP or (b) 5 mM pNPP in the presence of DMSO or 40 μM **6g**. Mean ± SEM % activity of PTPs incubated with inhibitors compared to DMSO is shown. The dotted line indicates 50% activity. Data from two independent experiments performed in triplicate are shown.

Hepatocyte Insulin Signaling. We next examined the efficacy of **6g** at inhibiting intracellular LMPTP activity. Since LMPTP inhibits insulin signaling in hepatocytes, we used phosphorylation of IR effector protein kinase B/AKT on activating residue Thr308 as a readout for LMPTP inhibition in human HepG2 hepatocytes. Treatment with 500 nM **6g** substantially increased HepG2 AKT Thr308 phosphorylation after insulin stimulation (Figure 6).

DIO Diabetes Model. We next examined whether treatment with **6g** would reverse high-fat diet (HFD)-induced diabetes in mice. We administered 0.03% (roughly equivalent to 30 mg/kg/day) **6g** in HFD chow to diabetic DIO mice for 2 weeks and assessed glucose tolerance and fasting insulin levels. Treatment with **6g** significantly improved glucose tolerance and decreased fasting insulin levels of diabetic DIO mice (Figure 7a,b). Concordantly, treatment with **6g** also resulted in increased insulin-stimulated phosphorylation of the IR activation motif and increased phosphorylation of AKT Thr308 in the livers of DIO mice (Figure 7c,d).

CONCLUSIONS

In conclusion, we have optimized a series of purine-based LMPTP inhibitors to give potent and orally bioavailable compounds. In this process, we have maintained selectivity for LMPTP against other PTPs and a unique uncompetitive MOA wherein the inhibitor binds to the opening of the LMPTP

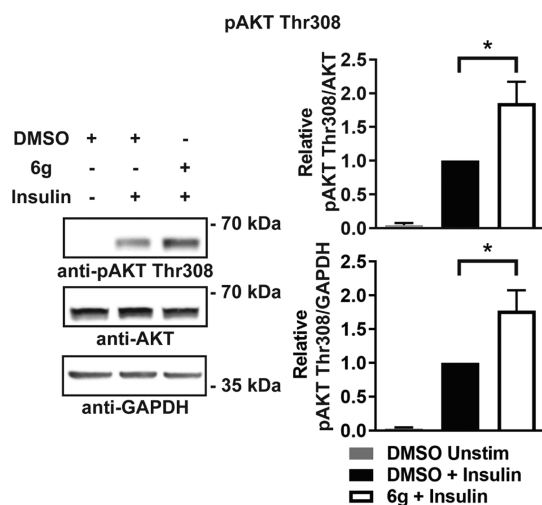


Figure 6. Compd **6g** augments insulin-stimulated AKT phosphorylation in hepatocytes. HepG2 hepatocytes were incubated overnight with DMSO or 500 nM **6g** solubilized in DMSO and stimulated with 10 nM insulin for 5 min or left unstimulated (Unstim). Left, representative western blots (cropped) of pAKT Thr308 from HepG2 cell homogenates. Right, quantification of pAKT Thr308/AKT and pAKT Thr308/GAPDH from eight independent experiments. Mean \pm SEM is shown. * $p < 0.05$, two-tailed unpaired t -test with Welch's correction.

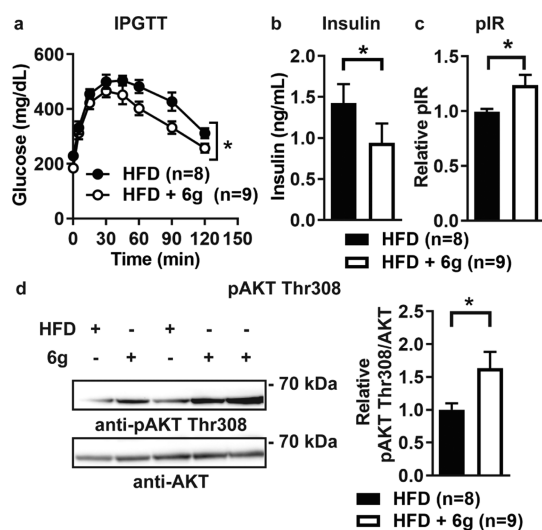


Figure 7. Oral administration of **6g** reverses diabetes and enhances liver insulin signaling in obese mice. DIO male B6 littermate mice were treated with 0.03% w/w **6g** in HFD or HFD alone for 2 weeks. (a) IPGTT. (b) Fasting plasma insulin levels of mice as assessed by ELISA. (c,d) Mice were injected intraperitoneally with insulin and livers harvested after 10 min. (c) IR tyrosine phosphorylation in liver homogenates was assessed by pIR ELISA. (d) pAKT Thr308 was assessed by western blotting of liver homogenates. Left, representative western blots (cropped). Right, quantification of pAKT Thr308/AKT. (a–d) HFD, $n = 8$; HFD + **6g**, $n = 9$. Mean \pm SEM is shown. * $p < 0.05$: (a) two-way ANOVA, (b) Mann–Whitney test, and (c,d) two-tailed unpaired t -test with Welch's correction.

active site to block completion of catalysis. This mechanism has not yet been reported for other PTPs. An orally bioavailable compound in this series attenuates insulin resistance and obesity-induced diabetes in mice, further substantiating the importance of LMPTP as a critical driver of insulin resistance and diabetes in obesity and the potential

for LMPTP inhibition as a therapeutic strategy for treatment of T2DM.

EXPERIMENTAL SECTION

All compounds were purified to >95% as determined by liquid chromatography (LC)–mass spectrometry (MS) as well as ^1H (and ^{13}C in select cases) NMR and high-resolution MS (HRMS). Reagents were purchased from Sigma-Aldrich unless otherwise noted. An example of a synthesis is shown below. The analytical methods, general chemistry, experimental information, and syntheses of all other compounds³¹ are supplied in the Supporting Information.

Synthesis of 8-(4-Chloro-phenyl)-3-(2,6-dichloro-benzyl)-3H-purin-6-ylamine (5c). Step a: to a mixture of adenine (2.2 g, 16.3 mmol) in water (200 mL) was added bromine (6.0 mL, 17.7 mmol) dropwise at rt. The resulting mixture was then stirred for 2 days at rt. The solvent and volatiles were removed in vacuo. The residue was washed with water (15 mL \times 2) and ethyl acetate (15 mL \times 2) to give 8-bromo-9H-purin-6-ylamine (2.1 g, yield: 60.3%) as a yellow solid. ^1H NMR (400 MHz, DMSO- d_6): δ 8.90 (br, 2H), 8.46 (s, 1H). ESI: calcd for $\text{C}_5\text{H}_4\text{BrN}_5$, 212.97. Observed m/z : $[\text{M} + \text{H}]^+$, 213.9. Step b: to a solution of 8-bromo-3H-purin-6-ylamine (3.1 g, 14.5 mmol) in dimethylformamide (DMF) (20 mL) was added 1,3-dichloro-2-chloromethyl-benzene (2.8 g, 14.5 mmol) and K_2CO_3 (4.0 g, 29.0 mmol). The reaction mixture was stirred at room temperature under N_2 overnight. The solvent was removed under vacuum. The residue was slurried with water (10 mL \times 3) and MeOH (10 mL \times 3), filtered, and dried under vacuum to give 8-bromo-3-(2,6-dichloro-benzyl)-3H-purin-6-ylamine (4c) (1.91 g, yield: 36%) as a yellow solid. ESI: calcd for $\text{C}_{12}\text{H}_8\text{BrCl}_2\text{N}_5$, 370.93. Observed m/z : $[\text{M} + \text{H}]^+$, 372.3. Step c: a flask charged with 8-bromo-3-(2,6-dichloro-benzyl)-3H-purin-6-ylamine (100 mg, 0.27 mmol), 4-chlorophenylboronic acid (84.0 mg, 0.54 mmol), K_2CO_3 (111 mg, 0.81 mmol), and Pd(dppf) Cl_2 (~20 mg, 20% wt) in dioxane (5 mL)/ H_2O (1 mL) was degassed and filled with N_2 . The reaction mixture was heated at 90 $^\circ\text{C}$ for 16 h. The solvent was removed and the residue was purified by preparative high-performance LC to give 8-(4-chloro-phenyl)-3-(2,6-dichloro-benzyl)-3H-purin-6-ylamine (25.0 mg, yield: 23%) as a white solid. ^1H NMR (400 MHz, DMSO- d_6): δ 8.22 (s, 1H), 8.15 (d, $J = 8.8$ Hz, 2H), 8.05 (br s, 2H), 7.56 (d, $J = 8.0$ Hz, 2H), 7.48–7.43 (m, 3H), 5.78 (s, 2H). HRMS: calcd for $\text{C}_{18}\text{H}_{12}\text{N}_5\text{Cl}_3$ $[\text{M} + \text{H}]^+$, 405.6884. Observed m/z : $[\text{M} + \text{H}]^+$, 405.6881. HPLC Purity: 99%.

Generation of Recombinant PTPs. Recombinant human LMPTP-A was purified as described.²³ Other PTPs used for selectivity assays were either purified or purchased as described in ref 23.

Enzymatic Assays. Phosphatase assays were performed in buffer containing 50 mM bis–tris, pH 6.0, 1 mM DTT, and 0.01% Triton X-100 at 37 $^\circ\text{C}$. For assays conducted with 3-*O*-methylfluorescein phosphate (OMFP) as substrate, fluorescence was monitored continuously at $\lambda_{\text{ex}} = 485$ and $\lambda_{\text{em}} = 525$ nm. For assays conducted with *para*-nitrophenylphosphate (*p*NPP) as substrate, the reaction was stopped by addition of 2 \times reaction volume of 1 M NaOH, and absorbance was measured at 405 nm. IC_{50} values were determined from plots of inhibitor concentration versus percentage of enzyme activity. For inhibitor selectivity assays, each PTP was incubated with either 0.4 mM OMFP or 5 mM *p*NPP in the presence of a 40 μM compound or dimethyl sulfoxide (DMSO).

Crystallization, Structure Solution, and Refinement. Crystals of LMPTP 4–157 in complex with **5d** grew by the sitting drop vapor diffusion method against a reservoir buffer containing 24–32% PEG 3350, 160 mM KNO_3 , and 100 mM bis–tris, pH 5.0. Crystals belong to space group $P2_12_12_1$ with unit cell parameters $a = 55.0$ \AA , $b = 59.0$ \AA , $c = 95.1$ \AA and two molecules per asymmetric unit. A native dataset extending to 1.3 \AA resolution and >99% complete to 1.4 \AA was collected at Stanford Synchrotron Radiation Lightsource beamline 12-2 and processed using HKL2000.³² The structure was solved by molecular replacement in PHASER³³ with the structure of human LMPTP (PDB ID 5JNR) as the search model. Coot³⁴ and reemac³⁵ were used for manual model building and refinement,

respectively. The final model contains residues 3–157 and 1–106, 109–157 for molecules A and B, respectively, with 424 solvent molecules and no residues in disallowed regions of the Ramachandran plot as assessed by Rampage.³⁶ Data collection and refinement statistics are summarized in Table S1. PDB ID 7KH8.

AKT Phosphorylation in HepG2 Cells. Human HepG2 cells (American Type Culture Collection [ATCC] catalogue #HB-8065) were cultured in Eagle's minimal essential medium (ATCC) containing 10% fetal bovine serum (FBS), 100 U/mL penicillin, and 100 µg/mL streptomycin. Cells were treated with DMSO or 500 nM **6g** in serum starvation media (0.1% FBS) overnight, following which cells were stimulated with 10 nM bovine insulin (Sigma) for 5 min at 37 °C in the presence of DMSO or 500 nM **6g**. For detection of AKT phosphorylation by western blotting, cells were lysed in 1× cell lysis buffer (Cell Signaling Technology; CST) with 1 mM phenylmethylsulfonyl fluoride (PMSF). Lysates were sonicated at 4 °C for 15 intervals of 10–15 s. Insoluble fractions were cleared by centrifugation. Prior to sodium dodecyl sulfate-polyacrylamide gel electrophoresis, protein concentrations of lysates were assessed using the Pierce BCA Protein Assay Kit (Thermo Scientific). Detection of AKT phosphorylation by western blotting was assessed using anti-phospho-AKT (pAKT) Thr308 (#4056) and anti-panAKT (#4691) antibodies (CST). Western blotting quantification was performed using ImageJ. Photo editing was performed using Adobe Photoshop.

Diabetes Assessment in DIO Mice. Animal experiments were conducted in accordance with the Animal Care and Use Committee-approved protocol at the University of California, San Diego (#S16098). B6 mice were purchased from Jackson Laboratory (JAX #000664) and bred in-house. To generate DIO mice, male littermates were fed HFD chow containing 60 kcal % fat (Research Diets) for 3 months starting at 1–2 months of age. DIO littermates weighing ≥35 g were assigned to treatment (HFD formulated with 0.03% w/w **6g**) or control (HFD alone) groups. After 2 weeks of treatment, mice were fasted overnight for 13 h, and intraperitoneal glucose tolerance test (IPGTT) was performed by administering 1 g glucose/kg body weight by IP injection. Tail ends were snipped 1 h before glucose injection. Blood glucose levels were obtained from a small drop of blood from tail snip right before glucose injection and at the indicated time points after glucose injection using a OneTouch glucometer. For insulin levels, mice were fasted overnight for 13 h and blood was collected from the facial vein. Plasma insulin levels were assessed using the Ultra-Sensitive Mouse Insulin enzyme-linked immunosorbent assay (ELISA) kit (Crystal Chem). To assess liver insulin signaling, fasted mice were injected IP with 10 U insulin (Eli Lilly)/kg body weight, and after 10 min mouse livers were harvested, flash-frozen, and homogenized in 1× cell lysis buffer with 1 mM PMSF. Homogenates were sonicated at 4 °C for 10 intervals of 30 s. Insoluble fractions were cleared by centrifugation. IR tyrosine phosphorylation was assessed using the PathScan phospho-IR (pIR) β (Tyr1150/Tyr1151) Sandwich ELISA Kit (#7258, CST). AKT Thr308 phosphorylation was assessed by western blotting as described above.

Statistical Analysis. All linear regressions, non-linear data fitting, and statistical analyses were performed using GraphPad Prism software. α values were determined by fitting of data to a mixed model of inhibition. K_i values were determined by fitting of data to an uncompetitive model of inhibition. The two-way analysis of variance (ANOVA), unpaired *t*-test with Welch's correction, and Mann-Whitney test were performed where appropriate as reported in the figure legends. A comparison was considered significant if *p* was less than 0.05.

■ ASSOCIATED CONTENT

SI Supporting Information

The Supporting Information is available free of charge at <https://pubs.acs.org/doi/10.1021/acs.jmedchem.0c02126>.

Experimental procedures and spectroscopic data for selected compounds, selectivity of **3** and **5d**, details of

the co-crystal structure with **5d**, details of the PK studies, MOA of **6g** (PDF)

SMILES molecular formula strings (CSV)

Accession Codes

The coordinates and diffraction data for the co-crystal structure described in this study have been deposited to the Protein Data Bank (www.rcsb.org) with ID 7KH8. Authors will release the atomic coordinates upon article publication.

■ AUTHOR INFORMATION

Corresponding Authors

Stephanie M. Stanford – Department of Medicine, University of California, San Diego, La Jolla, California 92037, United States; Phone: 01-858-246-2397; Email: ststanford@health.ucsd.edu

Nunzio Bottini – Department of Medicine, University of California, San Diego, La Jolla, California 92037, United States; Phone: 01-858-246-2398; Email: nbottini@health.ucsd.edu

Anthony B. Pinkerton – Conrad Prebys Center for Chemical Genomics, Sanford Burnham Prebys Medical Discovery Institute, La Jolla, California 92037, United States; orcid.org/0000-0003-4571-152X; Phone: 01-858-795-5320; Email: apinkerton@sbpdiscovery.org

Authors

Michael A. Diaz – Department of Medicine, University of California, San Diego, La Jolla, California 92037, United States

Robert J. Ardecky – Conrad Prebys Center for Chemical Genomics, Sanford Burnham Prebys Medical Discovery Institute, La Jolla, California 92037, United States

Jiwen Zou – Conrad Prebys Center for Chemical Genomics, Sanford Burnham Prebys Medical Discovery Institute, La Jolla, California 92037, United States

Tarmo Roosild – Conrad Prebys Center for Chemical Genomics, Sanford Burnham Prebys Medical Discovery Institute, La Jolla, California 92037, United States

Zachary J. Holmes – Department of Medicine, University of California, San Diego, La Jolla, California 92037, United States

Tiffany P. Nguyen – Department of Medicine, University of California, San Diego, La Jolla, California 92037, United States

Michael P. Hedrick – Conrad Prebys Center for Chemical Genomics, Sanford Burnham Prebys Medical Discovery Institute, La Jolla, California 92037, United States

Socorro Rodiles – Conrad Prebys Center for Chemical Genomics, Sanford Burnham Prebys Medical Discovery Institute, La Jolla, California 92037, United States

April Guan – Conrad Prebys Center for Chemical Genomics, Sanford Burnham Prebys Medical Discovery Institute, La Jolla, California 92037, United States

Stefan Grotegut – Conrad Prebys Center for Chemical Genomics, Sanford Burnham Prebys Medical Discovery Institute, La Jolla, California 92037, United States

Eugenio Santelli – Department of Medicine, University of California, San Diego, La Jolla, California 92037, United States

Thomas D. Y. Chung – Conrad Prebys Center for Chemical Genomics, Sanford Burnham Prebys Medical Discovery Institute, La Jolla, California 92037, United States

Michael R. Jackson – Conrad Prebys Center for Chemical Genomics, Sanford Burnham Prebys Medical Discovery Institute, La Jolla, California 92037, United States

Complete contact information is available at:
<https://pubs.acs.org/10.1021/acs.jmedchem.0c02126>

Author Contributions

This work represents a collaborative effort from Sanford Burnham Prebys Medical Discovery Institute (SBP) and the University of California, San Diego (UCSD) led by senior investigators from both institutions (A.B.P., S.M.S., N.B.). Investigators at SBP were primarily responsible for SAR studies and investigators at UCSD were primarily responsible for MOA, cell-based, and in vivo studies. All authors participated in preparing the manuscript.

Notes

The authors declare the following competing financial interest(s): Patent applications covering the compounds have been filed by SBP. N.B. and S.M.S. have equity interests in Nerio Therapeutics, a company that may potentially benefit from the research results, and receive income from the company for consulting. The terms of this arrangement have been reviewed and approved by the University of California, San Diego, in accordance with its conflict of interest policies.

ACKNOWLEDGMENTS

This work was supported by the National Institutes of Health grant R01 DK106233 to N.B. and A.B.P. S.M.S. was supported by the American Diabetes Association Pathway to Stop Diabetes Grant 1-15-INI-13.

DEDICATION

This paper is dedicated to the memory of our friend and colleague T.R. (1969–2019), an exceptional scientist and human being.

ABBREVIATIONS

ACPI, acid phosphatase 1; ANOVA, analysis of variance; B6, C57BL/6; BQL, below the quantification limit; Cl, drug clearance; C_{max} , peak plasma concentration; CST, cell signaling technology; DIEA, *N,N*-diisopropylethylamine; FBS, fetal bovine serum; Fig, figure; HFD, high-fat diet; HL, half-life; IP, intraperitoneal; IPGTT, intraperitoneal glucose tolerance test; IR, insulin receptor; LMPTP, low-molecular-weight protein tyrosine phosphatase; LYP, lymphoid phosphatase; mpk, mg/kg; MRT, mean residence time; ND, not detected; OMFP, 3-*O*-methylfluorescein phosphate; pAKT, phospho-AKT; pIR, phospho-insulin receptor/phospho-IR; PKB/AKT, protein kinase B; PMSF, phenylmethylsulfonyl fluoride; pNPP, *para*-nitrophenylphosphate; prep-TLC, preparative thin-layer chromatography; prep-HPLC, preparative high-performance liquid chromatography; PTP, protein tyrosine phosphatase; PTP1B, protein tyrosine phosphatase 1B; $R_{sq, adj}$, R -squared adjusted; SBP, Sanford Burnham Prebys Medical Discovery Institute; SD, standard deviation; SEM, standard error of the mean; SHP2, SH2 domain-containing phosphatase 2; T_{last} , time of last measurable concentration; T_{max} , time of maximum plasma concentration; UCSD, University of California San Diego; Unstim, unstimulated; $V_{d, ss}$, volume of distribution (steady-state); V_z , volume of distribution (elimination); VHR, vaccinia H1-related phosphatase

REFERENCES

- (1) Satteli, A. R. Putting the Brakes on Insulin Signaling. *N. Engl. J. Med.* **2003**, *349*, 2560–2562.
- (2) Boucher, J.; Kleinriders, A.; Kahn, C. R. Insulin Receptor Signaling in Normal and Insulin-Resistant States. *Cold Spring Harbor Perspect. Biol.* **2014**, *6*, a009191.
- (3) Stein, S. A.; Lamos, E. M.; Davis, S. N. A Review of the Efficacy and Safety of Oral Antidiabetic Drugs. *Expert Opin. Drug Saf.* **2013**, *12*, 153–175.
- (4) Satteli, A. R.; Kahn, C. R. Insulin Signaling and the Regulation of Glucose and Lipid Metabolism. *Nature* **2001**, *414*, 799–806.
- (5) White, M. F.; Shoelson, S. E.; Keutmann, H.; Kahn, C. R. A Cascade of Tyrosine Autophosphorylation in the Beta-Subunit Activates the Phosphotransferase of the Insulin Receptor. *J. Biol. Chem.* **1988**, *263*, 2969–2980.
- (6) Musi, N.; Goodyear, L. J. Insulin Resistance and Improvements in Signal Transduction. *Endocrine* **2006**, *29*, 73–80.
- (7) Johnson, T. O.; Ermoloeff, J.; Jirousek, M. R. Protein Tyrosine Phosphatase 1b Inhibitors for Diabetes. *Nat. Rev. Drug Discovery* **2002**, *1*, 696–709.
- (8) Stanford, S. M.; Bottini, N. Targeting Tyrosine Phosphatases: Time to End the Stigma. *Trends Pharmacol. Sci.* **2017**, *38*, 524–540.
- (9) Zeng, L.-F.; Zhang, R.-Y.; Yu, Z.-H.; Li, S.; Wu, L.; Gunawan, A. M.; Lane, B. S.; Mali, R. S.; Li, X.; Chan, R. J.; Kapur, R.; Wells, C. D.; Zhang, Z.-Y. Therapeutic Potential of Targeting the Oncogenic Shp2 Phosphatase. *J. Med. Chem.* **2014**, *57*, 6594–6609.
- (10) Krishnan, N.; Koveal, D.; Miller, D. H.; Xue, B.; Akshinthala, S. D.; Kragelj, J.; Jensen, M. R.; Gauss, C.-M.; Page, R.; Blackledge, M.; Muthuswamy, S. K.; Peti, W.; Tonks, N. K. Targeting the Disordered C Terminus of Ptp1b with an Allosteric Inhibitor. *Nat. Chem. Biol.* **2014**, *10*, 558–566.
- (11) Kerr, D. L.; Haderk, F.; Bivona, T. G. Allosteric Shp2 Inhibitors in Cancer: Targeting the Intersection of Ras, Resistance, and the Immune Microenvironment. *Curr. Opin. Chem. Biol.* **2021**, *62*, 1–12.
- (12) Li, K.; Hou, X.; Li, R.; Bi, W.; Yang, F.; Chen, X.; Xiao, P.; Liu, T.; Lu, T.; Zhou, Y.; Tian, Z.; Shen, Y.; Zhang, Y.; Wang, J.; Fang, H.; Sun, J.; Yu, X. Identification and Structure-Function Analyses of an Allosteric Inhibitor of the Tyrosine Phosphatase Ptpn22. *J. Biol. Chem.* **2019**, *294*, 8653–8663.
- (13) Caselli, A.; Paoli, P.; Santi, A.; Mugnaioni, C.; Toti, A.; Camici, G.; Cirri, P. Low Molecular Weight Protein Tyrosine Phosphatase: Multifaceted Functions of an Evolutionarily Conserved Enzyme. *Biochim. Biophys. Acta, Proteins Proteomics* **2016**, *1864*, 1339–1355.
- (14) Alonso, A.; Sasin, J.; Bottini, N.; Friedberg, I.; Friedberg, I.; Osterman, A.; Godzik, A.; Hunter, T.; Dixon, J.; Mustelin, T. Protein Tyrosine Phosphatases in the Human Genome. *Cell* **2004**, *117*, 699–711.
- (15) Alonso, A.; Nunes-Xavier, C. E.; Bayón, Y.; Pulido, R. The Extended Family of Protein Tyrosine Phosphatases. *Methods Mol. Biol.* **2016**, *1447*, 1–23.
- (16) Magherini, F.; Giannoni, E.; Raugei, G.; Cirri, P.; Paoli, P.; Modesti, A.; Camici, G.; Ramponi, G. Cloning of Murine Low Molecular Weight Phosphotyrosine Protein Phosphatase C α : Identification of a New Isoform. *FEBS Lett.* **1998**, *437*, 263–266.
- (17) Lucarini, N.; Antonacci, E.; Bottini, N.; Borgiani, P.; Faggioni, G.; Gloria-Bottini, F. Phosphotyrosine-Protein-Phosphatase and Diabetic Disorders. Further Studies on the Relationship between Low Molecular Weight Acid Phosphatase Genotype and Degree of Glycemic Control. *Dis. Markers* **1998**, *14*, 121–125.
- (18) Bottini, N.; Bottini, E.; Gloria-Bottini, F.; Mustelin, T. Low-Molecular-Weight Protein Tyrosine Phosphatase and Human Disease: In Search of Biochemical Mechanisms. *Arch. Immunol. Ther. Exp.* **2002**, *50*, 95–104.
- (19) Gloria-Bottini, F.; Gerlini, G.; Lucarini, N.; Borgiani, P.; Amante, A.; La Torre, M.; Antonacci, E.; Bottini, E. Phosphotyrosine protein phosphatase and diabetic pregnancy: an association between low molecular weight acid phosphatase and degree of glycemic control. *Experientia* **1996**, *52*, 340–343.

- (20) Iannaccone, U.; Bergamaschi, A.; Magrini, A.; Marino, G.; Bottini, N.; Lucarelli, P.; Bottini, E.; Gloria-Bottini, F. Serum Glucose Concentration and Acp1 Genotype in Healthy Adult Subjects. *Metabolism* **2005**, *54*, 891–894.
- (21) Bottini, N.; Gloria-Bottini, F.; Borgiani, P.; Antonacci, E.; Lucarelli, P.; Bottini, E. Type 2 Diabetes and the Genetics of Signal Transduction: A Study of Interaction between Adenosine Deaminase and Acid Phosphatase Locus 1 Polymorphisms. *Metabolism* **2004**, *53*, 995–1001.
- (22) Pandey, S. K.; Yu, X. X.; Watts, L. M.; Michael, M. D.; Sloop, K. W.; Rivard, A. R.; Leedom, T. A.; Mancham, V. P.; Samadzadeh, L.; McKay, R. A.; Monia, B. P.; Bhanot, S. Reduction of Low Molecular Weight Protein-Tyrosine Phosphatase Expression Improves Hyperglycemia and Insulin Sensitivity in Obese Mice. *J. Biol. Chem.* **2007**, *282*, 14291–14299.
- (23) Stanford, S. M.; Aleshin, A. E.; Zhang, V.; Ardecky, R. J.; Hedrick, M. P.; Zou, J.; Ganji, S. R.; Bliss, M. R.; Yamamoto, F.; Bobkov, A. A.; Kiselar, J.; Liu, Y.; Cadwell, G. W.; Khare, S.; Yu, J.; Barquilla, A.; Chung, T. D. Y.; Mustelin, T.; Schenk, S.; Bankston, L. A.; Liddington, R. C.; Pinkerton, A. B.; Bottini, N. Diabetes Reversal by Inhibition of the Low-Molecular-Weight Tyrosine Phosphatase. *Nat. Chem. Biol.* **2017**, *13*, 624–632.
- (24) Ardecky, R. J.; Hedrick, M. P.; Stanford, S. M.; Bliss, M. R.; Zou, J.; Gosalia, P.; Yamamoto, F.; Milewski, M.; Barron, N.; Sun, Q.; Ganji, S.; Mehta, A.; Sugarman, E.; Nguyen, K.; Vasile, S.; Suyama, E.; Mangravita-Novo, A.; Salaniwal, S.; Kung, P.; Smith, L. H.; Sergienko, E.; Chung, T. D. Y.; Pinkerton, A. B.; Bottini, N. Allosteric Small Molecule Inhibitors of LMPTP. *Probe Reports from the NIH Molecular Libraries Program*: Bethesda (MD), 2010.
- (25) Coussens, N. P.; Sittampalam, G. S.; Guha, R.; Brimacombe, K.; Grossman, A.; Chung, T. D. Y.; Weidner, J. R.; Riss, T.; Trask, O. J.; Auld, D.; Dahlin, J. L.; Devanaryan, V.; Foley, T. L.; Mcgee, J.; Kahl, S. D.; Kales, S. C.; Arkin, M.; Baell, J.; Bejcek, B.; Gal-Edd, N.; Glicksman, M.; Haas, J. V.; Iversen, P. W.; Hoepfner, M.; Lathrop, S.; Sayers, E.; Liu, H.; Trawick, B.; Mcvey, J.; Lemmon, V. P.; Li, Z.; McManus, O.; Minor, L.; Napper, A.; Wildey, M. J.; Pacifici, R.; Chin, W. W.; Xia, M.; Xu, X.; Lal-Nag, M.; Hall, M. D.; Michael, S.; Inglese, J.; Simeonov, A.; Austin, C. P. Assay Guidance Manual: Quantitative Biology and Pharmacology in Preclinical Drug Discovery. *Clin. Transl. Sci.* **2018**, *11*, 461–470.
- (26) Strelow, J.; Dewe, W.; Iversen, P. W.; Brooks, H. B.; Radding, J. A.; McGee, J.; Weidner, J. Mechanism of Action Assays for Enzymes. In *Assay Guidance Manual*; Sittampalam, G. S., Coussens, N. P., Nelson, H., Arkin, M., Auld, D., Austin, C., Bejcek, B., Glicksman, M., Inglese, J., Iversen, P. W., Li, Z., McGee, J., McManus, O., Minor, L., Napper, A., Peltier, J. M., Riss, T., Trask, Jr., O. J., Weidner, J., Eds.; Eli Lilly & Company and the National Center for Advancing Translational Sciences: Bethesda (MD), 2004.
- (27) Ring, B.; Wrighton, S. A.; Mohutsky, M. Reversible Mechanisms of Enzyme Inhibition and Resulting Clinical Significance. *Methods Mol. Biol.* **2014**, *1113*, 37–56.
- (28) Holdgate, G. A.; Meek, T. D.; Grimley, R. L. Mechanistic Enzymology in Drug Discovery: A Fresh Perspective. *Nat. Rev. Drug Discovery* **2018**, *17*, 115–132.
- (29) Pettersen, E. F.; Goddard, T. D.; Huang, C. C.; Couch, G. S.; Greenblatt, D. M.; Meng, E. C.; Ferrin, T. E. UCSF Chimera—a Visualization System for Exploratory Research and Analysis. *J. Comput. Chem.* **2004**, *25*, 1605–1612.
- (30) Wang, S.; Stauffacher, C. V.; Van Etten, R. L. Structural and Mechanistic Basis for the Activation of a Low-Molecular Weight Protein Tyrosine Phosphatase by Adenine. *Biochemistry* **2000**, *39*, 1234–1242.
- (31) Pinkerton, A. B.; Ardecky, R. J.; Zou, J. Inhibitors of Low Molecular Weight Protein Tyrosine Phosphatase (LMPTP) and Uses Thereof. WO 2019136093 A1, 2019.
- (32) Otwinowski, Z.; Minor, W. Processing of X-ray Diffraction Data Collected in Oscillation Mode. *Methods Enzymol.* **1997**, *276*, 307–326.
- (33) McCoy, A. J.; Grosse-Kunstleve, R. W.; Adams, P. D.; Winn, M. D.; Storoni, L. C.; Read, R. J. Phaser Crystallographic Software. *J. Appl. Crystallogr.* **2007**, *40*, 658–674.
- (34) Emsley, P.; Lohkamp, B.; Scott, W. G.; Cowtan, K. Features and Development of Coot. *Acta Crystallogr., Sect. D: Biol. Crystallogr.* **2010**, *66*, 486–501.
- (35) Murshudov, G. N.; Vagin, A. A.; Dodson, E. J. Refinement of Macromolecular Structures by the Maximum-Likelihood Method. *Acta Crystallogr., Sect. D: Biol. Crystallogr.* **1997**, *53*, 240–255.
- (36) Lovell, S. C.; Davis, I. W.; Arendall, W. B., 3rd; de Bakker, P. I. W.; Word, J. M.; Prisant, M. G.; Richardson, J. S.; Richardson, D. C. Structure validation by $C\alpha$ geometry: ϕ, ψ and $C\beta$ deviation. *Proteins* **2003**, *50*, 437–450.